Chapter 4

Warps and lags in the ionized and neutral hydrogen gas in the edge-on dwarf galaxy UGC 1281

Submitted to MNRAS

P. Kamphuis [1], R.F. Peletier [1], P.C. van der Kruit [1] and G.H. Heald[2]

[1] *Kapteyn Astronomical Institute,University of Groningen, Postbus 800, 9700 AV Groningen, the Netherlands*

[2] *ASTRON, 7990 AA Dwingeloo, the Netherlands*

Abstract

THE properties of the gas in halos of galaxies constrain global models of the interstellar medium. Kinematical information is of particular interest since it is a clue to the origin of the gas. Up-to now mostly massive galaxies have been investigated for their halo properties.

Here we report on deep HI and Hα observations of the edge-on dwarf galaxy UGC 1281 in order to determine the existence of extra planar gas and the kinematics of this galaxy. This is the first time a dwarf galaxy is investigated for its halo characteristics. We have obtained Hα integral field spectroscopy using PPAK at Calar Alto and deep HI observations with the WSRT of the edge-on dwarf galaxy UGC 1281. We have made a model for the 3D distribution of the HI in the galaxy.

We find that UGC 1281 has Hα emission up to 25$''$ (655 pc) in projection above the plane and in general a low Hα flux. Its HI extends 70$''$ (1.8 kpc) from the plane. This extra-planar gas can be explained either by a line of sight warp or in a lagging halo with a vertical rotational gradient of 8.7$\pm$4.1 km s^{-1} kpc^{-1}. Compared to other dwarf galaxies UGC 1281 seems to be a normal dwarf galaxy with a slowly rising rotation curve which flattens off to 60 km s^{-1} and a central depression in its HI distribution

4.1 Introduction

The discovery a very extended HI halo in NGC 891 has started a new field of halo kinematics. Since this discovery (Swaters et al. 1997) many investigations have followed studying this (Heald et al. 2006; Oosterloo et al. 2007) and other galaxies. These investigations have shown that NGC 891 is not a special case in having a halo (Schaap et al. 2000; Lee et al. 2001; Rossa & Dettmar 2003; Barbieri et al. 2005; Westmeier et al. 2005; Boomsma et al. 2005).

Theory has not yet converged on one explanation for the existence of these halos. Ideas range from internal gas brought up from the plane by galactic fountains (Shapiro & Field 1976; Bregman 1980) or chimneys (Norman & Ikeuchi 1989) to infalling primordial inter galactic gas (van der Hulst & Sancisi 1988, 2005). The biggest challenge for theory is to explain the 'lag' observed in the halo of NGC 891 and other galaxies.

In the halo of NGC 891 the gas higher above the plane is rotating slower . This 'lag' is observed in HI (Fraternali et al. 2005) as well as in Hα (Heald et al. 2006; Kamphuis et al. 2007a) and determined to be linear with a magnitude of $\sim$ 16 km s^{-1} kpc^{-1}.

Even though this lagging behavior is observed in other galaxies too, Heald et al. (2007) studied three other large galaxies and found a lag in all of them, it is not known whether it occurs in all halos. Until now, kinematical studies have focussed on massive galaxies and Low Surface Brightness (LSB) galaxies (Matthews & Wood 2003) but dwarf galaxies have not been observed yet in search of a halo or kinematic lag.

Besides the lag there are many other puzzles about dwarf galaxies and their gas content. One of the most interesting problems of dwarf galaxies is that they have slowly rising rotation curves and hardly display any differential rotation. This has led people to believe that these systems must be dark matter dominated in their center (Carignan & Freeman 1988; Swaters 1999). This would explain the shallow rise of the inner rotation curve and the lack of differential rotation (Côté et al. 2000).

Here we present deep HI and Hα observations of the edge-on dwarf galaxy UGC 1281 and analyze the kinematics of the HI and Hα in and above the plane. The 21 cm line emission was observed with the Westerbork Synthesis Radio Telescope (WSRT) and the Hα with the Integral Field Unit (IFU) PPAK on the 3.5 m telescope at Calar Alto.

The edge-on orientation of UGC 1281 provides us with an excellent opportunity to study the vertical structure of gas in a dwarf galaxy. Our HI observations of UGC 1281 are some of the deepest observations ever conducted on a dwarf galaxy, and never before has an edge-on dwarf galaxy been observed to this depth.

UGC 1281 is a nearby edge-on dwarf galaxy (M_B=-15.8, Swaters (1999)) with a systemic velocity of 156 km s^{-1} at a distance of 5.4 Mpc (Karachentsev et al. 2004). The galaxy has a angular diameter of 4.46 $'$ (D_{25}) (de Vaucouleurs et al. 1992) on the sky which would translate to 7 kpc at this distance. van Zee (2000) measured the star formation rate in UGC 1281 to be very low (0.0084 $M_\odot$ yr.$^{-1}$). These observations are supported by the non-detections in radio continuum (Hummel et al. 1991a) and IRAS. Indeed, Rossa & Dettmar (2003) observed UGC 1281 as a part of their extra-planar diffuse ionized gas (DIG) survey. They could not detect any extra-planar Hα in this dwarf galaxy, and concluded from this that UGC 1281 has a very low star formation rate.

Under the assumption that HI gas halos are created by processes related to star formation, little to no halo is expected when the SFR is low (though,due to the weak potential, gas might easily escape from the disk of the galaxy). However, in a dwarf galaxy,

Parameter	Value
Observation dates	2004 September
Total length of observation (hr)	4× 12
Velocity center of band (km s^{-1})	156
Total bandwidth (MHz)	10
Channels in obs.	1024
Channel sep. in obs. (kHz)	9.77
Channels in final cube	61
Vel. res. after Hanning smoothing (km s^{-1})	8.24

Table 4.1: Log of the HI observations

like UGC 1281, most of the baryonic material is thought to come from cold accretion (Kereš et al. 2005). Therefore, if halos are formed through accretion one would expect halos in dwarf galaxies.

This article is structured as followed. In § 4.2 and § 4.3 we will describe the observations and the data reduction, respectively. § 4.4 will contain the results of observations followed by a presentation of our models in § 4.5. We will discuss our results in § 4.6 and summarize in § 4.7

4.2 Observations

The 21 cm line emission, or HI observations, were obtained with the WRST during four nights in september 2004. In total 4 complete 12 hr observations were performed using the Maxi-Short configuration. This configuration gives the optimum performance for imaging extended sources. This is because it provides a good sampling of the inner $u-v$ plane with a shortest base line of 36 m. The longest baseline is 2754 m. An overview of the observational parameters is given in Table 4.1.

The Hα was observed with the PPAK integral field unit on the 3.5 m telescope at Calar Alto (Kelz et al. 2006). Three positions were observed in one night (see Table 4.2). At each position several exposures were taken. Two positions were observed for 3× 1200 s (North and Center) and one for 3× 600 s (South). The lower exposure time of the Southern field was due to twilight. The pointings of the North and South fields were shifted by $\sim \pm 76''$, compared to the Center, along an axis with a PA slightly offset ($\sim 10^\circ$ offset) from the PA of the galaxy. This was done to ensure a good coverage of extra-planar Hα. The spectra cover a wavelength range $\sim$ 5500-7000 Å with a resolution of 4.1 Å(187 km s^{-1} at Hα). The conditions were partially photometric with a mean seeing of $1.3''$, which is much less than the fiber size, which is $2.7''$.

4.3 Data Reduction

4.3.1 Radio data

The data reduction of the HI was done with the MIRIAD package (Sault et al. 1995). Care was taken not to include data affected by solar or other interference. Before and

Parameter	Field 1&2	Field 3
Name	North&Center	South
Observation dates	2006 September	same
Exposure time (s)	3600	1800
Central wavelength (Å)	6273	6273
Total bandwidth (Å)	1628	1628
Channels in obs.	1050	1050
Channel sep. in obs. (Å)	1.55	1.55
Channels in final cube	61	61
Channel separation (km s^{-1}) at Hα	70.8	70.8

Table 4.2: Log of the Hα observations

Parameter	Full Res.	Circ. beam	Low Res.
Spatial resolution (arcsec)	25.0×13.4	26.0×26.0	60.0×60.0
Beam size (kpc)	0.65×0.35	0.68×0.68	1.57×1.57
rms noise per channel (mJy $beam^{-1}$)	0.44	0.50	0.72
Min. detectable col. dens. (3σ; cm^{-2})	7.1×10^{19}	4.0×10^{19}	1.1×10^{19}

Table 4.3: Parameters of the HI Data Cubes

after each 12 hr observation a calibration source (3C147 and CTD93) was observed, thus enabling us to determine the spectral response of the telescope. During each 12 hr observation no additional (phase) calibration sources were observed, as is standard practice with the WRST. Due to the large bandwidth, the time variations can be determined from self-calibration of a continuum image constructed from the channels free of line emission.

After the reduction and calibration additional analysis was performed with the GIPSY package (van der Hulst et al. 1992). The final cube was reduced to 61 velocity channels with a velocity spacing of 4.12 km s^{-1}, which results in a velocity resolution after Hanning smoothing of 8.24 km s^{-1}. The original cube has a spatial resolution of $25.0'' \times 13.4''$. This cube was smoothed to two cubes with circular beams of $26''$ (0.68 kpc) and $60''$ (1.57 kpc) to avoid beam orientation effects and to detect low level emission (See Table 4.3). The position of the center of the galaxy, as determined by Swaters (1999) from *R*-band photometry, was set to zero in the three cubes and they were rotated by 50 ° (PA = 40°, Swaters (1999)) to orient the major axis of the galaxy parallel to the x-axis of the image.

4.3.2 IFU data

For the reduction of the PPAK spectra the IRAF package was used. Basically the steps in the `dohydra` Guide (Valdes 1995) were followed manually to ensure complete control over the reduction. We traced the apertures on the science frames themselves. This caused no problems since there was enough continuum emission in each spectrum.

For the initial wavelength calibration 7 lines of a HeNe+ThAr lamp were used. After

this initial wavelength calibration the fine tuning calibration was done with 5 sky lines in each science frame. For the sky line subtraction all sky fibers of each frame were checked for inconsistencies. Except for sky fibers with the galaxy in their field of view, no inconsistencies were found and the remainig 95 sky fibers were used for the subtraction of the skylines.

After the reduction and calibration the different exposures of each field were combined by calculating the median of the separate exposures. No clipping was applied. The three fields were then positioned into one field by overlaying the continuum images of the fields on top of a *R*-band DSS image. By taking special care that the five stars in the three fields were aligned properly, this procedure resulted in a position error of $1''$, which is smaller than the $2.7''$ fiber size.

Our reduced and calibrated data were further analyzed with a combination of IDL programs produced by the SAURON collaboration (e.g. de Zeeuw et al. (2002)) and ourselves. The data were Voronoi binned with the voronoi_2d_binning IDL program (Cappellari & Copin 2003) to obtain a higher S/N ratio (S/N > 20). Like the HI, the central position of the galaxy was set to (0,0) and the galaxy was rotated by 50° to align the major axis with the x-axis.

4.4 Results

For display purposes, all of the regions in the data without signal are masked in the figures presented in this paper. For the HI this was done by smoothing the cube to a circular beam of $60''$ and then using the values above 3 σ as a mask for the cube with a circular beam of $26''$. In case of the Hα the bins without emission are simply taken away from the data and thus not displayed.

4.4.1 Gas distribution

Here, we first discuss the distribution of the ionized gas and then the HI gas distribution. In Section 4.6 we will compare the two distributions, highlight the differences and similarities, and discuss possible interpretations of these distributions.

Hα Distribution

Figure 4.1 shows the Hα flux obtained with the PPAK IFU instrument. This map was constructed by displaying the log of the peak obtained by fitting a Gaussian to the binned spectra. All the fitted Gaussians were inspected by eye, and none of the fitted lines showed significant deviations from Gaussian. Overlaid on the image are the contours of an integrated HI moment map.

The first thing we see from Figure 4.1 is that the ionized hydrogen is mostly located in 5 or 6 distinct peaks but that there is low level emission almost everywhere in the central field of view. The distinct peaks can most likely be associated with large HII regions in the galaxy whereas the low level emission is indicating a diffuse ionized component. The two innermost peaks at the NE and SW side of the center of the galaxy might be caused by a ring structure in the distribution. This seems to be implied by their equal distance from the center but they might also just be normal HII regions.

A warp is clearly seen in the HII regions as well as the diffuse emission. The peak of

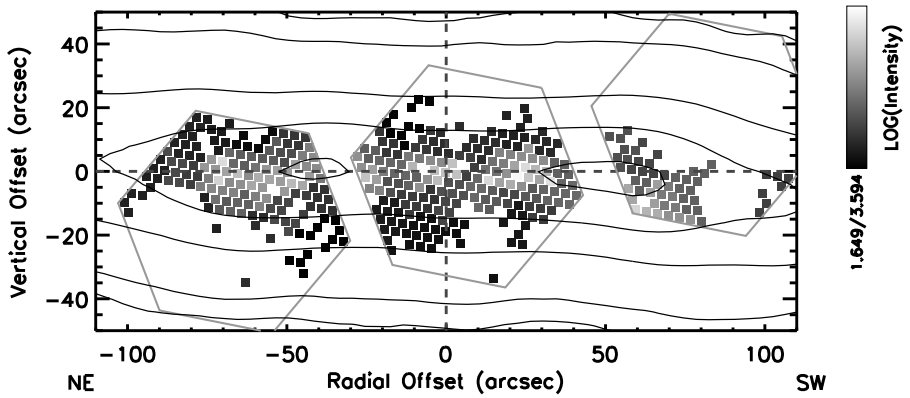

Figure 4.1: Integrated Hα flux map of UGC 1281. The map was constructed by taking the log of the height of the fitted Gaussian in each spectrum and the position were rotated by 50° . The red lines indicate the full field of view of the PPAK observations. Overlaid in black are the contours of an integrated HI moment map. The contours are at 1.5, 3, 6, 12, 24, 48, 96, 192, 273 σ levels of the data where $\sigma = 2.2$ mJy/beam. Color version on Page 132.

the emission starts to deviate from the major axis at a distance from the center of about 50″ (1.3 kpc). In the South West (SW) of the galaxy we see an exception to this behavior with a large ionized hydrogen peak below the major axis, where the diffuse emission still seems to be mostly on the major axis. This seems to indicate an HII region that is either somewhat offset from the plane or located in the outskirts of the galaxy. If the warp axis is not exactly perpendicular to the line of sight the outer parts will not only experience a change in position angle but also in inclination. Thus if this HII region is located in the outskirts of the galaxy its position can still be in the warped plane of the galaxy.

In our data the maximum vertical extent of the diffuse gas, detected from the major axis in UGC 1281, is $\sim 25''$ (0.65 kpc). This is similar to the the extent of the stars ($\frac{1}{2}d_{25,minor} = 18''$, van Zee (2000), $\frac{1}{2}d_{25,minor} = 23''$, de Vaucouleurs et al. (1992)). If we fit an exponential to the inner vertical intensity profile of the ionized gas we find a scale height of 8.5″ (0.22 ± 0.03 kpc) assuming that the galaxy is seen perfectly edge-on. When we follow the same procedure for the continuum emission in our spectra and an I-band image (obtained through the NASA extragalactic database) we find a scale height of 7.6″ (0.20 ± 0.01 kpc) and 8.0″ (0.21 ± 0.01 kpc) respectively.

The Hα data is so irregular that making a model for comparison will not bring more insight into the structure of the Hα distribution. Also, the distribution is peaked in many places whereas our models would resemble a smooth exponential distribution. However, there are several parameters that can be derived from the data or obtained from the literature. They are presented in table 4.4 for comparison to the HI model.

HI Distribution

Figure 4.2 shows the DSS 2 blue image of UGC1281. Overlaid are the contours of our integrated HI flux map of UGC 1281. This map was constructed by adding all channels

Parameter	Value	Reference
Scale height	0.22 ± 0.03 kpc	[1]
Scale length	1.09 kpc	[2]
SFR	0.0084 $M_\odot$ yr. $^{-1}$	[2]
Hα luminosity	$3.81 \pm 0.01 \times 10^{-13}$ erg s^{-1} cm^{-2}	[3]

Table 4.4: Hα parameters that could be measured from the observations or obtained from the literature. [1] this chapter [2] van Zee (2001) [3] van Zee (2000)

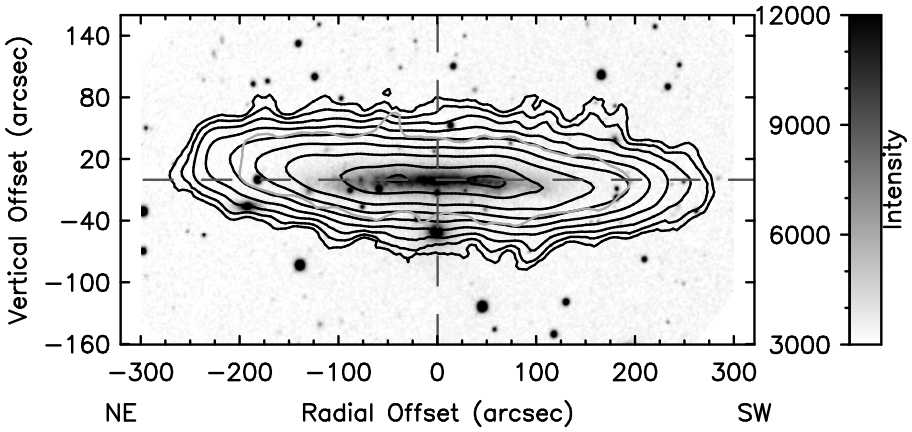

Figure 4.2: Continuum image in the blue from the DSS 2 overlaid with contours of our integrated HI flux map of UGC 1281. The map was constructed by first smoothing the original cube to a circular beam of 60″ . This smoothed cube was used to mask the original cube. The mask was set to 3 σ of the 60″ cube. Then all channels of the masked unsmoothed cube were added and the image was rotated by 50 °. The black contours are the same as in Fig. 4.1. The red contour indicates the 3σ contour of the WHISP observations. Color version on Page 132.

from the masked 26″ cube. From Figure 4.2 we can see that the HI of UGC 1281 is at first glance quite symmetrically and evenly distributed. A closer look reveals asymmetries and peculiarities in the HI distribution. It warps away from the major axis at about 90″ (2.4 kpc) on the South West and at about 100″ (2.6 kpc) on the North East. The warp is not symmetric at all and seems to wiggle or form a w shape. Especially at the South West side there seems to be a return towards the major axis. The highest projected deviation from major axis is 6°. This warp was already observed by García-Ruiz et al. (2002) in the WHISP observations of this galaxy.

When we compare the lowest contour in the integrated moment map of the WHISP observations with our own (See fig. 4.2, red contour), we see that in our observations more emission is detected in the radial as well as in the vertical direction. The growth in both directions is similar extent and this indicates that even with our deep observations we might not be detecting the lowest levels of emission of this galaxy.

Furthermore, the HI distribution displays a central depression. This depression ap-

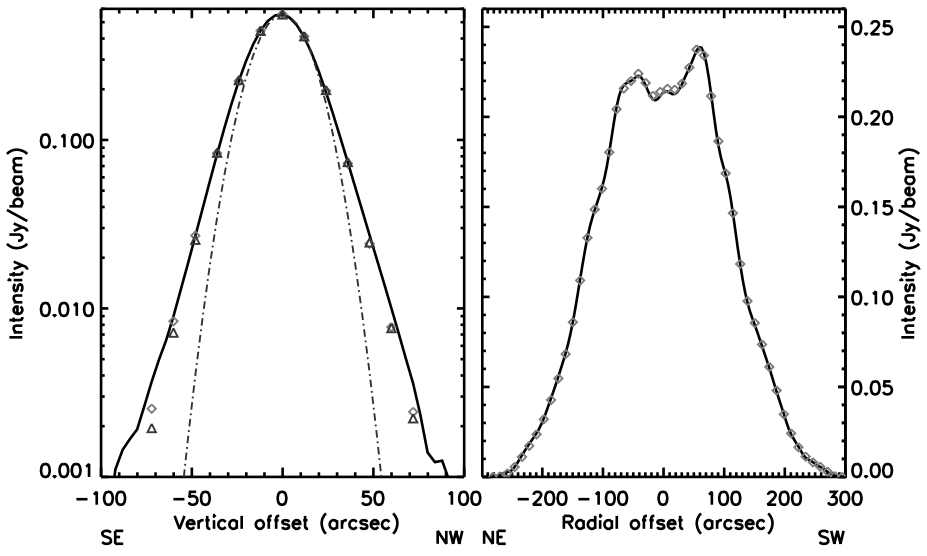

Figure 4.3: Intensity profiles of the observed HI. Left figure: Vertical intensity profile, averaged over the inner 100″ in the radial direction. Right figure: Radial intensity profile, averaged over the inner 40″ of the galaxy in the vertical direction. Black line: Data, Red diamonds: Halo model, Blue triangles: Maximum warp model, Blue dashed-dotted line: beam. Color version on Page 133.

pears as a ring around the center of the galaxy. The depression ranges from 10″ to 40″ (0.26-1.05 kpc) radial offset from the center of the galaxy. It is symmetrical around the center of the galaxy even though it is much deeper on the NE side of the galaxy.

The HI in UGC 1281 shows significant extensions away from the major axis. The HI extends up to 70″ (1.8 kpc) on both sides of the plane at column densities $N_{HI} = 4.0 \times 10^{19}\mathrm{cm}^{-2}(3\sigma)$. This extent is much more than the FWHM of the beam (26″) which is clearly seen in Figure 4.3, in which the vertical distribution of the data and a Gaussian with a FWHM of 26″ is shown. We see that the wings of the data are much more extended than the observational beam. This outer part of the HI distribution can easily be fitted with one exponential with a scale height of 12.4″ (0.32 kpc).

If the vertical extent of the HI is to be explained by an inclination of the outer rings, this inclination would be $\sim 75°$, assuming an infinite thin disk, i.e. deviating from the inclination of the inner disk by 15° . Although not impossible if the warp is almost exactly along the line of sight, the w shape in the position angle makes it unlikely that we actually see the warp exactly along the line of sight. This is because in a regular warp, the PA and inclination of every ring would be related to each other. In a warp in the plane of the sky such a warp would translate to a pure change in PA. In the opposite case, of a warp purely along the line of sight, it would translate completely into a change

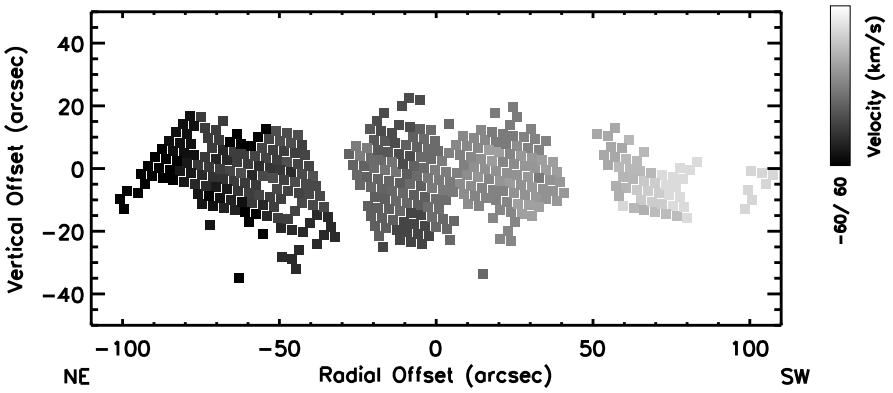

Figure 4.4: Velocity field of the ionized gas. The field was constructed by taking the central position of the fitted Gaussian in every spectra. The systemic velocity ($v_{sys} = 156.$ km s^{-1}) has been set to 0. The separate pixels show the fiber positions and the colors run from -60 to 60 km s^{-1}. Color version on Page 132.

of inclination. In between these two orientations the warp would be a combination of changing inclination and PA, with the weights of the two depending on the orientation of the actual warp axis. Therefore, in UGC 1281 the small wiggles ($< 6°$) in PA would translate into huge jumps in inclination ($> 10°$) from beam to beam if the warp were to be almost along the line of sight. This seems unphysical for a semi-stable system. Therefore we assume that the warp axis is not tilted by more than 45° from the plane of the sky. In this case the change in inclination in the outer parts cannot be large enough to fully explain the wings in the vertical profile. Of course it is always possible that UGC 1281 is not a semi-stable system or that the warp is highly irregular. In these cases the vertical extent of the HI might be explained by a warp, but then the apparent symmetry and regularity of the rest of the system has to be explained.

4.4.2 Velocity Distribution

Hα Velocities

Figure 4.4 shows the velocity field of the PPAK observations. This velocity field was obtained by fitting a gaussian to each emission line, with the IDL routine GAUSSFIT, and taking its peak position as the velocity in that fiber. This is by no means equal to the actual deprojected maximum rotational velocity in the galaxy but it is an apparent mean velocity determined by a combination of the rotational velocity, the density distribution of the ionized gas, and the opacity of the dust. From here on whenever we mention velocity we are referring to this mean velocity unless otherwise noted. The gaussian fitting procedure, and therefore the mean velocity, was chosen because with a channel separation of 70 km s^{-1} it is impossible to confidently fit the intrinsic shape of the emission line.

Figure 4.5 (left) shows a cut 10″ wide of the velocity field along the major axis.

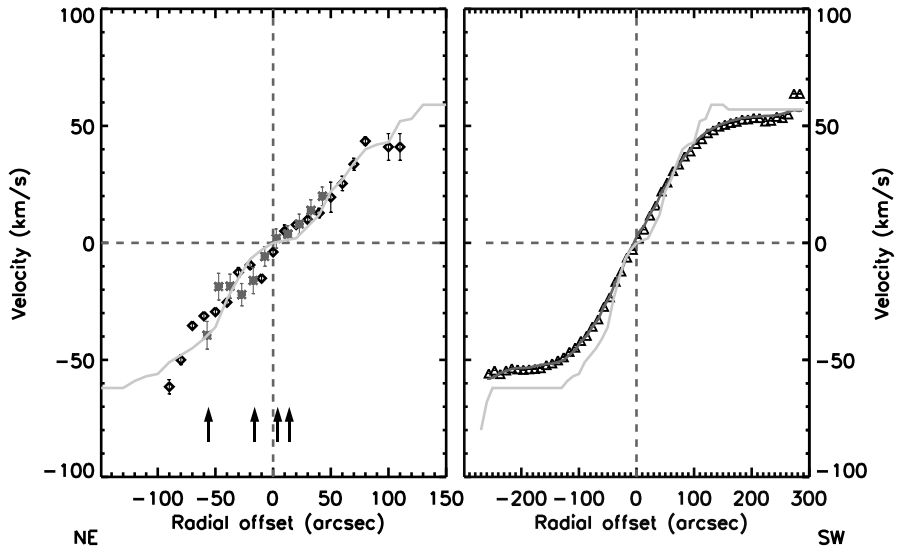

Figure 4.5: Velocities along the major axis. The left panel shows the Hα velocities: Black symbols are the PPAK data presented in this paper, Blue symbols are the data obtained by Kuzio de Naray et al. (2006). Right figure shows HI velocities: Black symbols are the HI, The blue line shows the velocities obtained from the model. The red line is the input unprojected rotation curve of the intermediate warp model described in § 4.5. The arrows indicate the positions of the velocity cut parallel to the minor axis in Figure 4.6. Color version on Page 133.

In this plot we see clearly that the part of the galaxy observed in our Hα field of view is still resembling a slow rising rotation curve that indicates solid body rotation. This behavior of the rotation curve is quite typical for dwarf galaxies, which all seem to have a large inner region in which their rotation curve resembles solid body rotation (Côté et al. 2000).

Another thing that is quite clear is that the peaks in the Hα along the major axis do stand out in the velocity curve as HII regions should. This indicates that most of the peaks we see in the Hα distribution are indeed HII regions. Another explanation is that the intensity peaks correspond to a higher density in the radial density profile of the galaxy with thicker clumps offset from the line of nodes. This explanation is supported by the fact that they appear symmetrically around the center of the galaxy (see Section 4.4.1) and that the star formation rate in UGC 1281 is so low (SFR = 0.0084 $M_\odot$ yr.$^{-1}$) that giant HII regions would not be expected to reside in the galaxy .

Figure 4.5 also shows the velocities obtained by Kuzio de Naray et al. (2006) with the DensePAK IFU for UGC 1281. They were not able to trace emission as far out in radius with their observations. Since their exposure time and fiber size is equal to ours this is

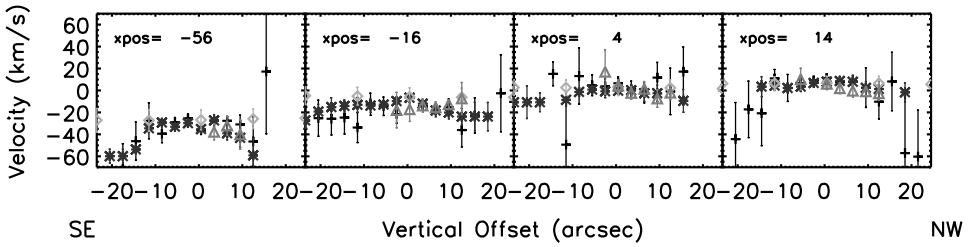

Figure 4.6: Four cuts parallel to the minor axis through the velocity field at **-56, -16, 4, 14**″ radii offset from the center. The negative (positive) offsets are the South East (North West) in the sky. Black points are the, unbinned PPAK data. Blue, voronoi binned PPAK data. Red, HI data. Green, Kuzio de Naray et al. (2006) data. Color version on Page 133.

most likely caused by the fact that they do not bin the data and the lower sensitivity of the DensePak IFU. The velocities obtained by Kuzio de Naray et al. (2006) lie on the top of our values within the errors, which ensures us that there are no systematic errors in our reduction or the gaussian fitting procedure.

The velocities of the ionized gas above the plane are at first glance somewhat peculiar. Instead of corotation or a lag, UGC 1281 actually shows higher rotation above the plane. It seems unlikely that the gas above the plane is rotating faster than the gas in the plane. Therefore, an orientational explanation, which lowers our velocities on the major axis, is preferable to a physical explanation. This drop could be caused by giant HII regions in the plane of the galaxy. Their position is offset from the line of nodes and therefore they lower our velocity measures as can also be seen in Figure 4.5.

This 'dipping' behavior is illustrated in Figure 4.6. These plots show the velocity as function of vertical offset from the plane in bins 10″ wide for the binned and unbinned Hα (blue and black,respectively), the data from Kuzio de Naray et al. (2006) (green), and the HI (red). We see that also above the major axis, the DensePak data and our data agree within the errors. In Figure 4.6 the velocities move away from the systemic velocity above the plane. When we look at the rotation curve (Figure 4.5) at the radial offset of these plots we see that they are at a position where the rotation curve shows a drop in the velocities. Thus confirming the idea that the velocities drop towards the major axis. A more extended discussion will follow in Section 4.6.2 in combination with the results of the HI.

HI Velocities

Figure 4.7 shows the velocity field of the HI observations. This velocity field was constructed with the MOMENTS routine in GIPSY by selecting the first moment of the masked data cube. The routine determines the intensity weighted mean velocity position of the peak of the line profile in every pixel of the cube. For symmetric profiles, this is analogous to fitting a gaussian profile to the emission line and taking its velocity at the peak. Since our galaxy has only small rotational values the line profiles are almost symmetric. We have checked this by comparing a map with the velocities where the line profiles have their maximum with this GIPSY map and we find no differences greater than

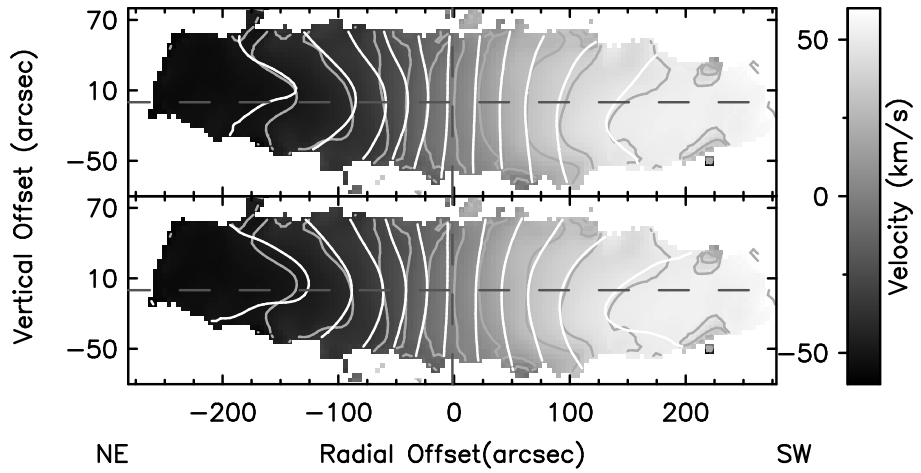

Figure 4.7: Velocity field of the neutral hydrogen. The field was constructed with the task MOMENTS in GIPSY (see text). Contours are from -60 km s^{-1} to 60 km s^{-1} with increasing steps of 10 km s^{-1} Black contours are the data. The white contours in the upper panel show the maximum warp model without a lag. In the lower panel the white contours show the best fit intermediate warp-halo model with a lag of 8.7 km s^{-1} kpc^{-1} (See § 4.5). Color version on Page 134.

6 km s^{-1}, which is within our errors. Thus, these velocities are in principle comparable one to one with the velocities of the Hα and differences should be due to the conditions of the gas (distribution effects, dust, resolution, self absorption, or a real difference in the rotational speed of the ionized and neutral gas).

Figure 4.5 (right) shows a cut 10″ wide of the velocity field along the major axis. Here we see the same slow rise in the rotation curves as seen in the Hα but we also see that in the HI we do reach the flat part of the rotation curve at $\sim$ 120″ offset, outside the Hα field of view, from the center of the galaxy at a maximum velocity $\sim$ 60 km s^{-1} .

If we move away from the plane (Figure 4.7 and 4.8) we see that the velocities are lower than on the major axis. This implies that either the outer parts of the galaxy are heavily inclined, that the disk is flaring or that the gas above the plane is 'lagging'. We can measure this apparent lag in normalized PV-diagrams (See (Kamphuis et al. 2007a), § 6.2) parallel to the minor axis such as Figure 4.8 by fitting a straight line to the maxima between 20″ and 50″ offset from the plane. Of course this measurement is affected by the warp and beam smearing and possibly other systematics. Therefore, this value has to be compared to the same measurements of models that can explain this apparent lag. These models will be presented in the next Section and discussed in Section 4.6.

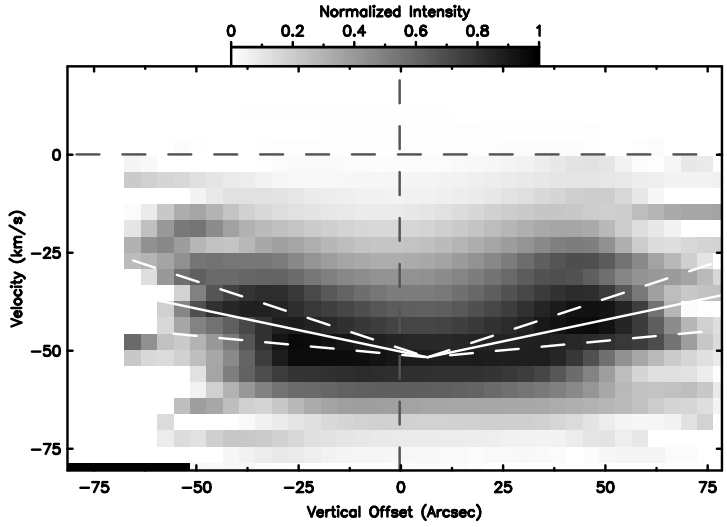

Figure 4.8: Normalized PV-diagram parallel to the minor axis averaged over 100″ at a radial offset of -175 to -75. The solid lines show the lag obtained from a halo model (See § 4.6.2). The dashed lines show the error on the lag. The zero point is set to the point of maximum intensity in a non-normalized PV diagram. Color version on Page 135.

4.5 Models

4.5.1 Tilted ring model

The modeling of the HI was done using a version of the GIPSY GALMOD routine modified by one of us (G. H.) and F. Fraternali which includes radial and vertical motion and a lag of the halo. The modeling is not straightforward, since many different parameters may be independently fitted. All of the parameters are fitted from the outside in. This is important, since small changes in density in the outer rings can seriously effect the inner rings as a result of the edge-on orientation of our galaxy. Since it is clear that the warp is not symmetric at all, we fit both sides of the galaxy independently.

An additional constraint is placed on the fitting procedure by the fact that we are dealing with a semi-stable system and so large jumps in inclination and position angle are not to be expected. We therefore do not allow the PA or inclination to change by more than 10° from one ring (10″) to the next .

The procedure followed for the fitting is iterative. We start by comparing radial and vertical density profiles of the data with the models. This has to be done to get a initial guess of the density profile. When these profiles have a reasonable fit we start fitting the position angle on a integrated moment map. The peak value at any radius in the integrated moment map should have the same offset from the plane in the models as in the data.

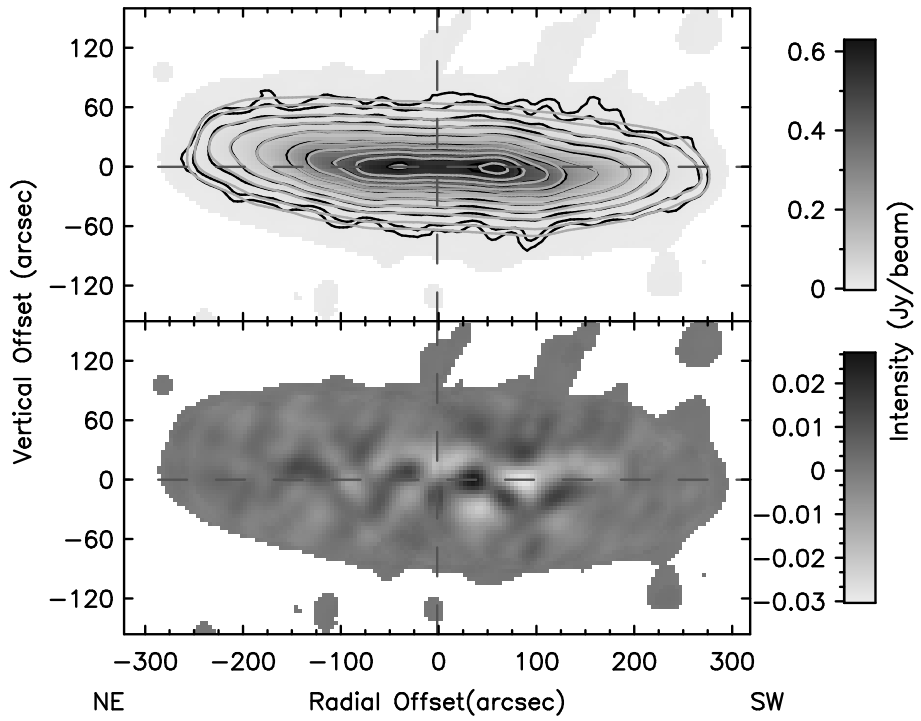

Figure 4.9: Upper panel: Integrated HI flux map of UGC 1281 (See Figure 4.2). The black contours are the Data at levels as in Figure 4.1. The red contours are the same levels for the best fit intermediate warp halo model. Lower panel: Residual map of the data minus the best fit model (total intensity). Color version on Page 134.

The inclination of each ring is related to the position angle when we assume a simple warp which is not completely in the line of sight. This fact is used to constrain the inclination of the rings. At this stage we split our modeling into two parts. One model has a warp which has a warping axis at an intermediate angle (45°) to the line of sight. The other model has a maximum line of sight warp. This maximum is set at the point where either the difference in inclination between two rings becomes larger than 10° or where the vertical profile starts to show a break, which is not observed in the data. Both these criteria are no longer satisfied if the angle between the line of sight and the warp axis becomes smaller than 35°.

When the comparison between the integrated moment map of the models and the data is to our satisfaction we proceed. Figure 4.3 shows how the density distribution of the intermediate warp model (red diamonds) compares to the density distribution of the data (black solid lines) on the major axis (right panel) and the minor axis (left panel). The blue dot-dashed line indicates the spatial resolution (FWHM = 26″). The left panel in Figure 4.3 also shows the vertical profile of the maximum warp best fit model (blue triangles).

As a last check on the density distribution we construct an integrated moment map of the residual cube. Figure 4.9 shows the residual map of the best fit density distribution.

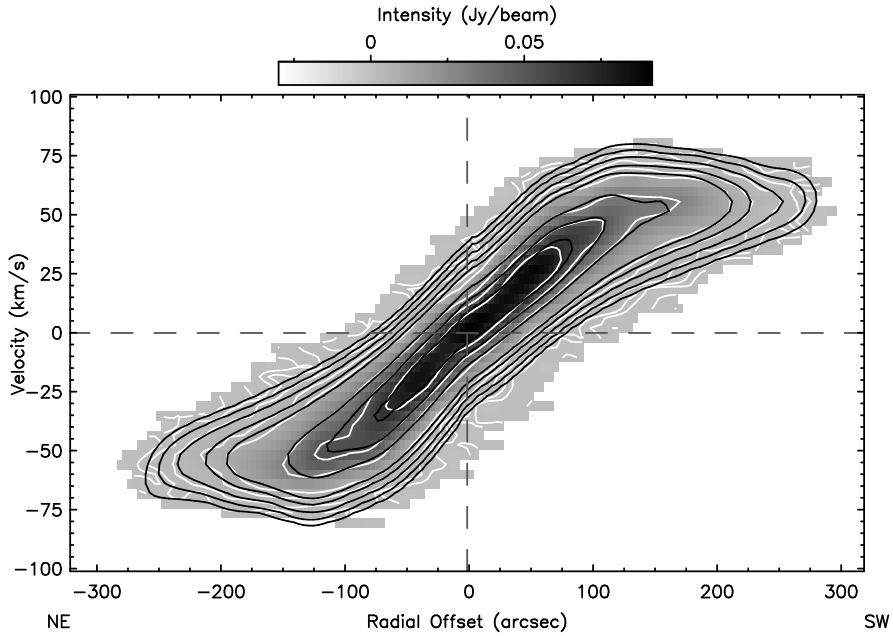

Figure 4.10: Color plot of the HI PV diagram along the major axis. Overlaid with contours of the data (white) and the best fit model (black). The contour levels are 1.5σ, 3σ and 6σ ($1\ \sigma = 0.5$ mJy/beam) etc. Color version on Page 135.

This figure shows only the density distribution of the best fit intermediate warp model because the differences in the density distribution between the two models is less than 5% everywhere in models that are masked in the same way as the data. Therefore the difference between these two models would not be visible in these plots.

We also constructed a model with a warp purely in the in the plane of the sky. Such a model with a constant inclination of 90° could not produce a satisfactory fit to the density.

After we obtain a satisfactory density distribution we start fitting the rotation curve and dispersion of the gas. As a first guess for the rotation curve we use the velocities from the Hα and HI. For the inner $\pm\ 50''$ we use the Hα velocities as our initial rotation curve. Beyond this point we use the velocities obtained from the HI first moment map (See Fig. 4.5).

Starting from this initial rotation curve we compare the model to the data. Again this is an iterative process that goes from the outside in. The fitting is done by first comparing the major axis Position Velocity (PV) diagram of the data to the model. This is shown in Figure 4.10, where the best fit intermediate warp model is plotted with the data. The color scheme and the white contours are the data whereas the black contours display our best fit intermediate warp model. Once more only the intermediate warp model is shown because also in this PV-diagram the differences between the two models are less than 5%.

When this PV-diagram is fitted correctly, the model cubes should now be compa-

Model	Flare	Warp	Lag	Good Fit?
Model A	Y	N	N	N
Model B	Y	N	Y	N
Model C	N	Y	N	N
Model D1	N	Y	Y	Y
Model E	Y	Y	N	N
Model D2	Y	Y	Y	Y
Model F	Y	Y	N	Y

Table 4.5: Models for high latitude emission. The columns show from left to right: The model name, Flared model, Warp included, Lagging model, fits the data.

rable to the data cube everywhere and any major deviations can only be caused by the galaxy's vertical velocity parameters deviating from the model. This could be caused by e.g. a lag, flaring or radial inflows. For this reason, we construct several models with different lags ranging from 0 to 16 km s^{-1} kpc^{-1}.

To exclude flaring, we also construct several models with and without flaring. All of these models are based on the best fit models and only differ in their flaring, lagging and warping properties. The different models are listed in Table 4.5 and PV-diagrams parallel to the minor axis are presented in Figure 4.11.

Figure 4.12 shows the parameters for the best fit models of UGC 1281 (Model D2 (black lines) & F (symbols)). The best fit for the intermediate warp model has a flare which would have an average scale height of 11.15″ (0.29 kpc) and a scale length of 46″ (1.2 kpc). This scale length is the same for the maximum warp model, which is also flaring with an average scale height of 9″ (0.22 kpc).

4.5.2 Ballistic Models

To investigate what we would expect for UGC 1281 in the sense of extra planar gas we have used the ballistic model of Collins et al. (2002). In this model gas is blown out of the disk into the halo by supernovea, with an initial vertical velocity (called the kick velocity). The model naturally predicts a vertical gradient in rotational velocity which has a higher magnitude in model with a high kick velocity. To obtain the vertical gradient of the model we follow the procedure outlined by Heald et al. (2007). The initial disk for the model is infinitely thin, this is because the scale height of the Hα in UGC 1281 is already comparable to the scale height normally used for the initial disk (0.2 kpc). Therefore this model should be thought of as an absolute upper limit on the kick velocity.

We find that the scale height of 0.2 kpc is reproduced when the initial kick velocity is 10 km s^{-1}. We run the simulation until the system reaches steady state ($\sim$ 1 Gyr). At this point there are no clouds in the halo at radii smaller than 4 kpc due to the radial outward movement of the clouds. Therefore we cannot measure the vertical gradient in the rotational speed at these radii. However, at radii between 5-10 kpc we find a small gradient of 0.4 km s^{-1} kpc^{-1}. This is a very low value as one would expect for a small galaxy like UGC 1281 since kick velocities must be small in a low potential, because otherwise the scale height becomes too large.

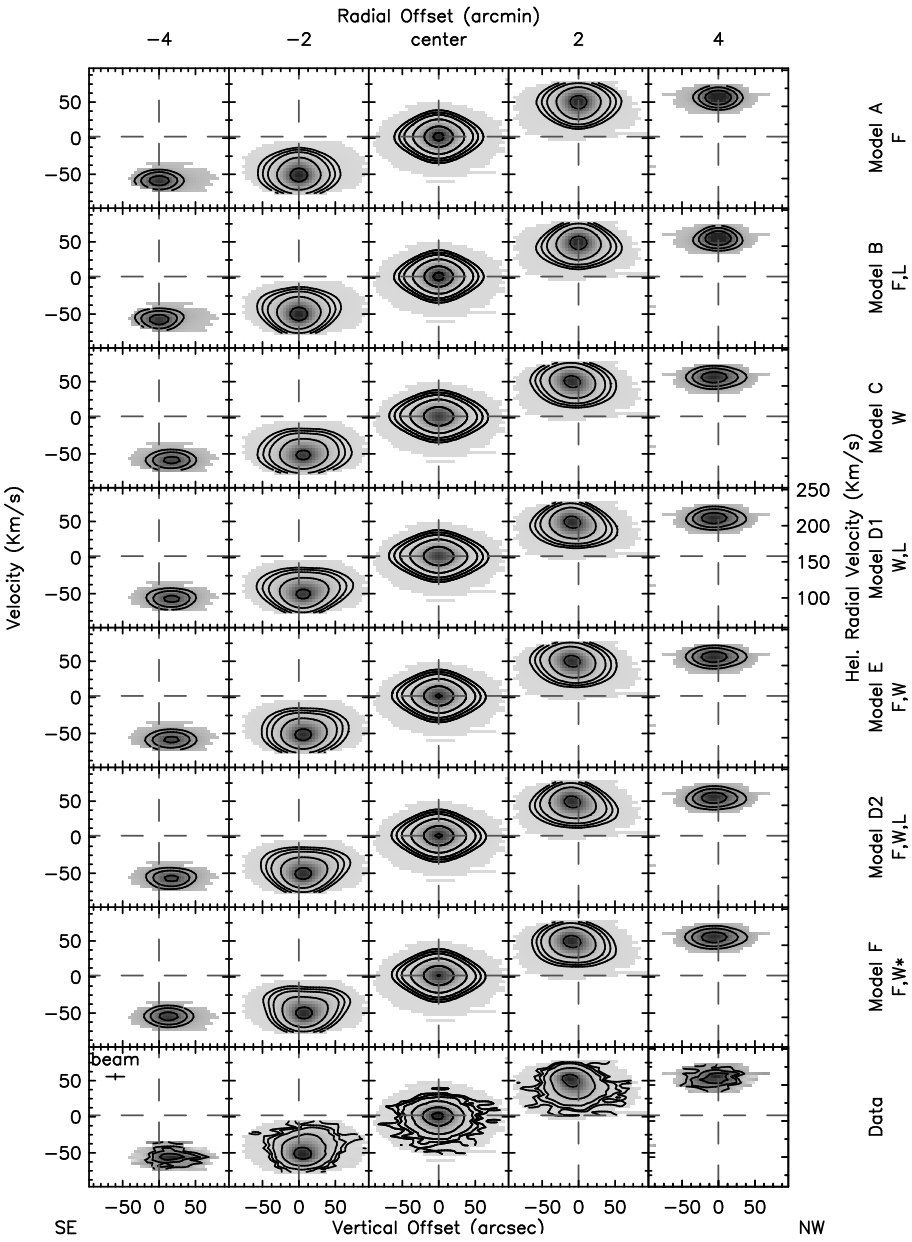

Figure 4.11: PV diagrams for the data and various models along the minor axis (center panel) and parallel to the minor axis 4' (outer panels) and (-)2' (2nd and 4th panel) away from the center. Contours are 1.5σ, 3σ, 6σ, 12σ (σ = 0.5mJy/beam). After 12σ the contours are from 10,40,80 mJy/beam. From top to bottom the rows are Model A, B ,C ,D1,E , D2, F and the bottom row shows the data. Below the model names we denote a general indication of the model where F stands for a flare, L for a vertical rotational gradient and W($*$) for an intermediate (maximum) line of sight warp. Color version on Page 136.

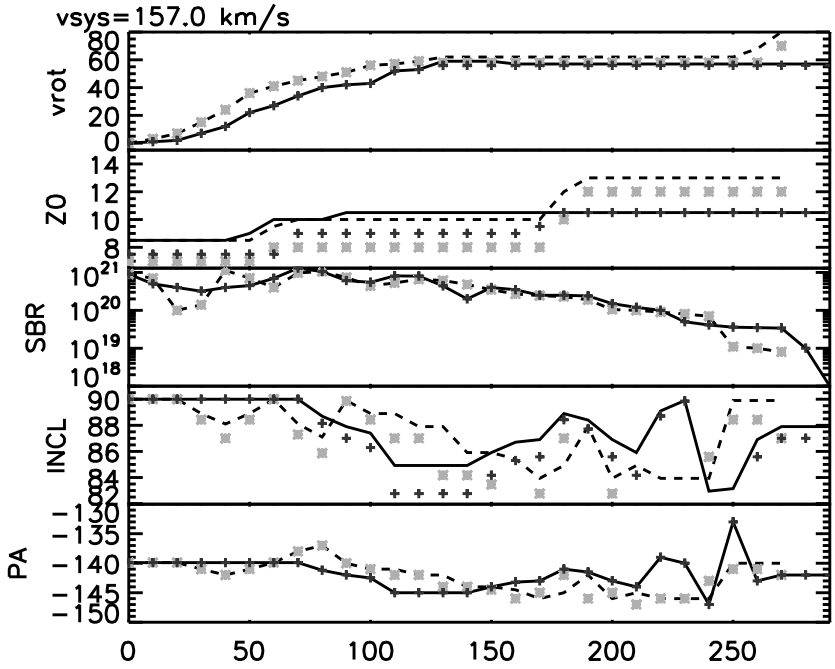

Figure 4.12: Model parameters as function of radius. For model D2 (Solid line: South West side, Dashed line: North East side) and Model F (Blue plusses: South West side, Red crosses: North East side). Color version on Page 139.

4.6 Discussion

4.6.1 Hydrogen in the plane

When we compare the parameters of the best fit HI models to the parameters extracted from the Hα data (Table 4.4) we see that compared to the ionized gas the neutral gas is much more extended in the radial direction. Apart from this its scale length is slightly larger. So, the ionized gas is more centrally concentrated than the HI.

Note that both the neutral gas and the ionized gas display a central depression in their distribution. Also, the Hα distribution is more irregular than the neutral hydrogen. This can easily be seen in Figures 4.1 and 4.2 by counting peaks in the distribution (see Section 4.4.1). One of these 'peaks' in Hα has a clear offset from the plane of the galaxy and this region does not stand out in the HI observations.

Another effect is the start of the warp. If we look at the integrated moment maps the neutral gas starts to deviate from the major axis at a radius almost two times larger than the radius where the Hα bends away from the major axis ($50''$ and $90''$, respectively). Most likely this is a resolution effect, because when we look at the best fit model for the HI we see both the HI and the Hα start to warp around $50''$ (1.3 kpc).

When we compare the measured velocities of the neutral and ionized gas they look very similar on the major axis (see Fig. 4.5). Ideally this should only occur if the sizes

of both disks are similar and there is no absorption, self-shielding or clumpiness affecting the emission. We know from the analysis of the Hα that the velocities in the plane are lower than those above the plane in several places. Also, the HI velocities are lower, due to beam smearing, when compared to the best fit model. Since, for the Hα emission we can only look at the rising part of the rotation curve, where the rotational velocities are low, deviations from the real rotational velocities are small. Therefore, it is not unreasonable that both effects provide us with the same velocities since all absolute deviations from the rotational velocities are small.

On the major axis the velocities in the Hα are higher than the HI velocities in the outer parts ($\sim 70''$ radial offset) of our PPAK observations. This fact seems to imply that the velocities in Hα are lowered by an observational effect that is most severe in the center of the galaxy. This is to be expected when there is dust, self shielding or when there are HII regions present.

The latter option is very attractive since we had already seen that the intensity distribution of the Hα shows several peaks which could be caused by HII regions. Also, we see clear variations in the velocity that indicate deviations from the rotational velocity (see Fig 4.5), most likely caused by giant HII regions or clumpiness in ring like structures. A less likely explanation is that there is either dust or Hα self-shielding in the plane of the galaxy. This is unexpected since the amount of Hα emission coming from the galaxy is low, and therefore high column densities are not to be expected. In the case of dust, no clear dust lane is observed, but UGC 1281 is observed to have a redder color than most dwarf galaxies (Makarova & Karachentsev 1998). This could, however, be solely caused by its high inclination.

Figure 4.5 (Red line) shows us that the real rotation curve is indeed slowly rising and reaches a flat part around 60 km s^{-1}. UGC 1281 has the slow rising rotation curve which is so common in dwarf galaxies, but it also shows clear differential rotation.

4.6.2 Hydrogen above the plane

We see (Figure 4.1) that the Hα extends less far in the vertical direction than the HI. Despite the fact that a difference in sensitivity may cause us to miss Hα emission at distances further from the plane than $20''$, the scale height, measured by fitting a single exponential to the vertical distribution, of the Hα is two thirds that of the HI scale height (0.2 kpc and 0.3 kpc, respectively).

Due to the small extent of the Hα above the plane, we cannot learn about its kinematics there. However, Figure 4.6 shows clearly that above the plane the Hα velocities are higher than in the plane of the galaxy. If these were real rotational velocities this would mean than the Hα above the plane is rotating faster, but as explained in the previous section this effect is most likely caused by HII regions in the plane that artificially decrease the measured velocities on the major axis.

We note that there is a discrepancy of $\sim$ 50 km s^{-1} between the velocity of the Hα and the HI above the plane, at a radial distance of -56$''$ from the center (left panel Figure 4.6). Because the maximum velocity derived from the HI model is 60 km s-1, this seems too much to be explained by dust absorption, self-shielding or inhomogenity. It is more likely that these velocities are affected by foreground emission in the Milky Way. A strong indication of this foreground emission is already given by the fact that in the

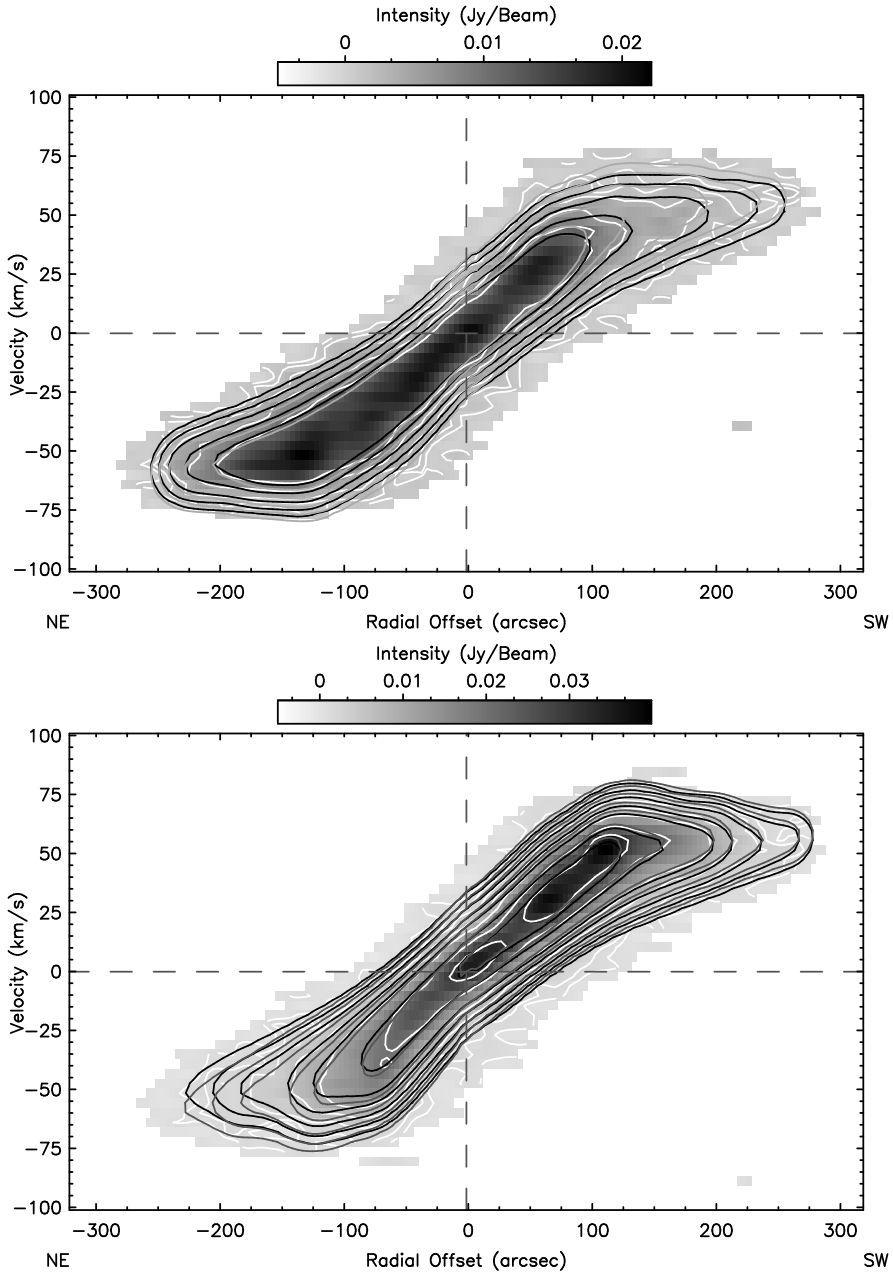

Figure 4.13: Top (Bottom): Color plot of the HI PV-diagram at 26 (-26)″ (±0.6 kpc) offset from the major axis. Contours are at 1.5 σ, 3 σ, 6σ and so on. The white solid contour is the data, red contour is the best fit model with no lag, black contour is the best fit model with an assumed vertical gradient of 8.7 km s^{-1} kpc^{-1} in the rotation curve. The colormap ranges are indicated above the panel in Jy/beam. Color version on Page 137.

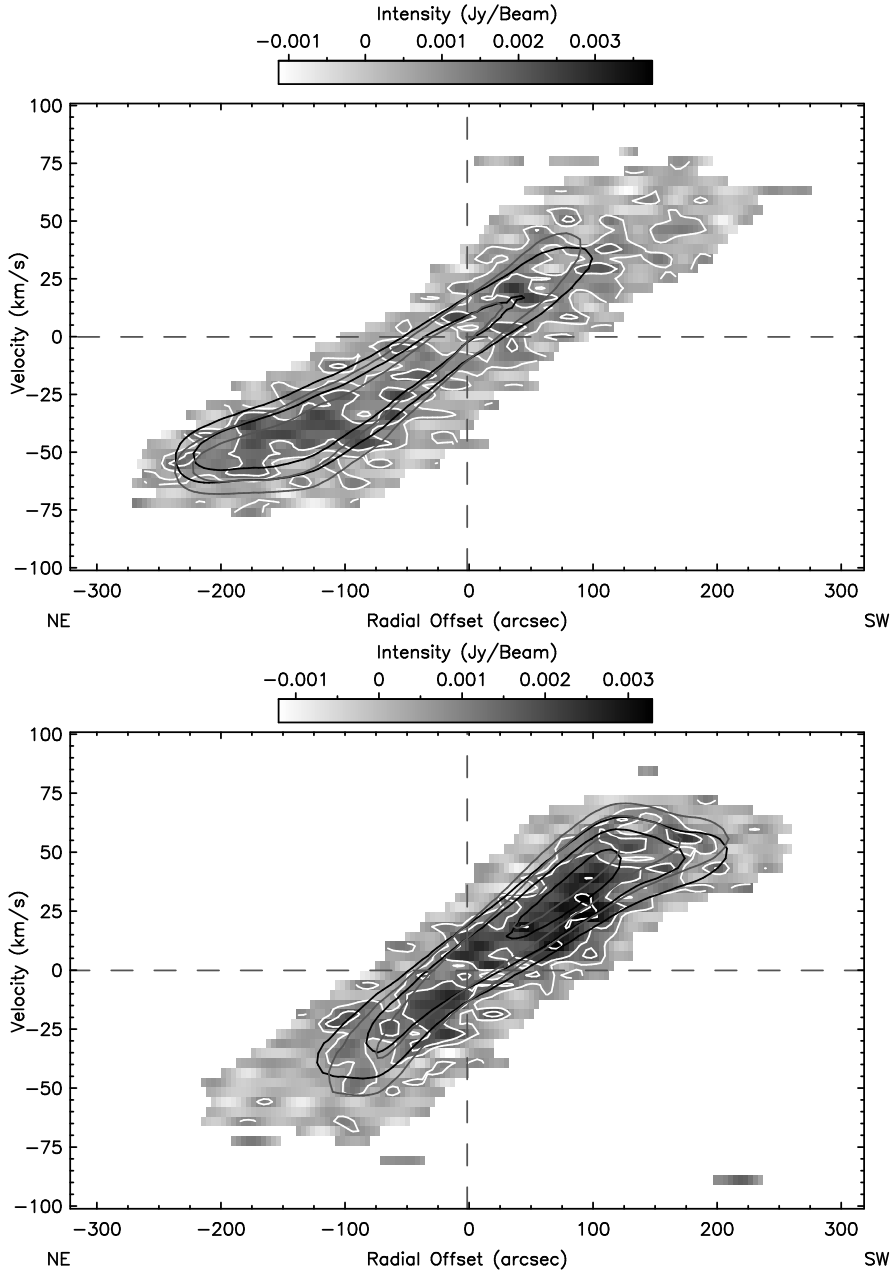

Figure 4.14: Same as Figure 4.13 but now at ± 56″ (±1.3 kpc) offset from the plane. Color version on Page 138.

North field one of our bins was excluded from the data because the emission had a negative heliocentric velocity of -46 km s^{-1}. Since this is only one FWHM from the velocities measured in the vertical velocity profile at an offset of -66″ , it seems a likely contaminator. Indeed when we look at the Leiden-Dwingeloo all sky survey (Hartmann & Burton 1997) we see that a small HI peak is present at heliocentric velocities of -50 km s^{-1} at our field of view. Moreover the intensity seems to be varying over our field of view. The fact that there is HI in the Milky Way at this position does not necessary mean there is also Hα but our bin with negative velocity does seem to imply this is so.

Even though the Hα is not supplying much information above the plane we can learn a lot about the kinematics above the plane from the HI. Figures 4.13 and 4.14 show PV-diagrams parallel to the major axis at ± 26 and ± 56″ offset from the plane. The first thing we see from these figures is the clear asymmetry between cuts above and below the plane. This asymmetry is caused by the warp of the galaxy.

Any further interpretations of these figures need a comparison with the models. From our modeling we obtain two possible explanations for the extra planar HI. We find that the model where we push the warp as much into the line of sight as the data allows (Model F) fits the data equally well as a model with a small lagging halo and a warp which is at an intermediate angle to the line of sight (Model D). We will discuss these two options and their implications in two separate sections below.

A lagging halo

In the case of a warp which is only partly in the line of sight (Model D) it turns out that the scale height of the HI is larger than that of the stars and the ionized hydrogen. This would indicate that if a halo is formed by galactic fountains the ionized gas would recombine before it reaches its maximum height above the plane. Another explanation for the smaller extent of the Hα could be that a halo is formed from infalling neutral gas.

We can measure the vertical lag present in the galaxy by fitting straight lines to the maxima in the normalized PV-diagrams parallel to the minor axis (See § 4.4.2) in the data and the models. We find that the value measured from the data corresponds to a lag of 8.7 ± 4.1 km s^{-1} kpc^{-1} (See Fig 4.15) in the intermediate warp model. With this lag there is no need to incorporate other changes into the models to get a satisfactory fit at all heights for this model. This way we obtain a lag of 8.7 ± 4.1 km s^{-1} kpc^{-1}.

Figures 4.13 and 4.14 show the contours for the best fit model without lag (red) and with a lag of 8.7 km s^{-1} kpc^{-1} (black). Already Figure 4.13 is indicative that a model with a lag gives a better fit, though we cannot exclude the non-lagging model at this height. At a height $\sim 60''$ above the plane (Fig. 4.14) it is clearly seen that the velocities around the 3σ contours are too high in the non-lagging model. Figure 4.11 also shows that the observed shapes in PV diagrams parallel to the minor axis indicate a thickening on the side of the systemic velocity (set to 0 km/s in Figure 4.11). If we compare this to the different models it is easily seen that only a lagging halo or a lagging flare (D1 and D2, respectively) can properly reconstruct the observed PV-diagrams parallel to the minor axis if the warp is not at its maximum line of sight alignment.

In this case there would be extra-planar gas that is lagging in velocity with respect to the disk with a vertical gradient of 8.7 ± 4.1 km s^{-1} kpc^{-1}. Even though a model with a warp with constant inclination of 90° can not produce a satisfactory fit to the data's

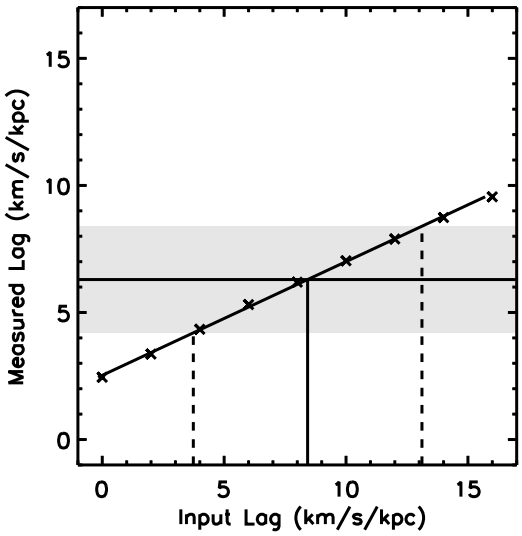

Figure 4.15: Input lag vs. Measured lag in the models. The solid line shows the fit to the measured values (displayed by crosses) of the models. The horizontal solid line displays the value obtained from the data. The vertical solid line shows where the measured value intersects the model fit. The grey shaded area indicates the error in the measurement and the dashed vertical lines where the error intersects the fit. This range determines the error bar on the value of the lag.

intensity distribution, it produces a velocity field similar to that of the intermediate warp model with a vertical velocity gradient of 0 km s^{-1} kpc^{-1}. We therefore ran this model also with a vertical velocity gradient of 8.7 $\pm$ 4.1 km s^{-1} kpc^{-1}, which again produced a velocity field similar to the one obtained from the best fit model. Thus, we believe that if this galaxy has a lagging halo the vertical gradient can at maximum be 8.7 $\pm$ 4.1 km s^{-1} kpc^{-1}.

As in the case of the super-thin galaxy UGC 7321 (Matthews & Wood 2003) the origin of the lagging HI extra-planar gas in a Low Surface Brightness (LSB) dwarf galaxy, with low star formation rates, would be puzzling.

Heald et al. (2007) have compared the lag, or the vertical gradient in the rotation curve in three massive galaxies. They find tentative evidence that when they scale the lag with the observed Hα scale height * this new parameter (dV/dh_z) is roughly constant at about 20 km s^{-1} scale height^{-1}. However, the galaxies compared are of similar mass. The results presented in this paper give us now the opportunity to look at a class of galaxies with much lower mass. The dynamical mass of UGC 1281 is 5.9×10^9M$_\odot$, measured at our last point of the rotation curve, as opposed to $\sim 1 \times 10^{11}$M$_\odot$ for the other galaxies (See Fig 4.16).

When we multiply the lag in UGC 1281 with its electron scale height we find dV/dh_z = 3.4 $\pm$ 0.9 km s^{-1} per scale height . This value is inconsistent with a constant dV/dh_z $\sim$ 20 km s^{-1} which was found for the 3 massive galaxies (see Fig 4.17). This is most

* Note that Heald et al. (2007) use electron scale heights instead of the emission measure scale heights.

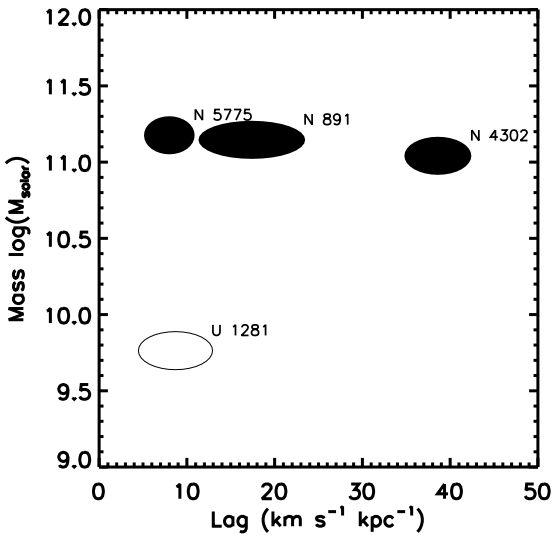

Figure 4.16: Vertical Lag vs. the log of the dynamical mass for the galaxies from Heald et al. (2007) (filled ellipses) and UGC 1281 (open ellipse). The horizontal axis of an ellipse indicates the error in lag for a specific galaxy

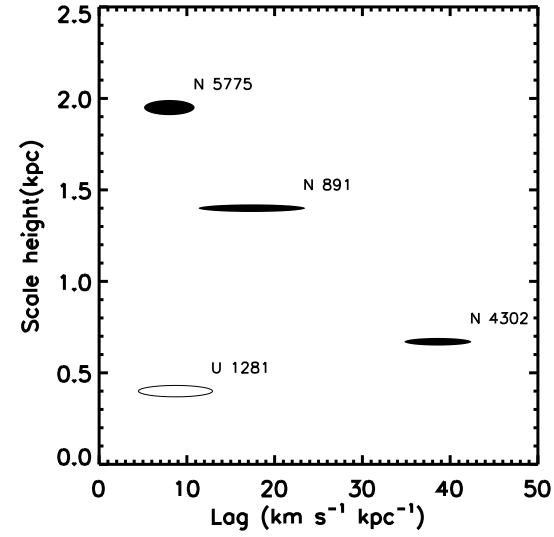

Figure 4.17: Vertical Lag vs. Hα scale height for the galaxies from Heald et al. (2007) (filled ellipses) and UGC 1281 (open ellipse). The horizontal (vertical) axis of an ellipse indicates the error in lag (scale height) for a specific galaxy

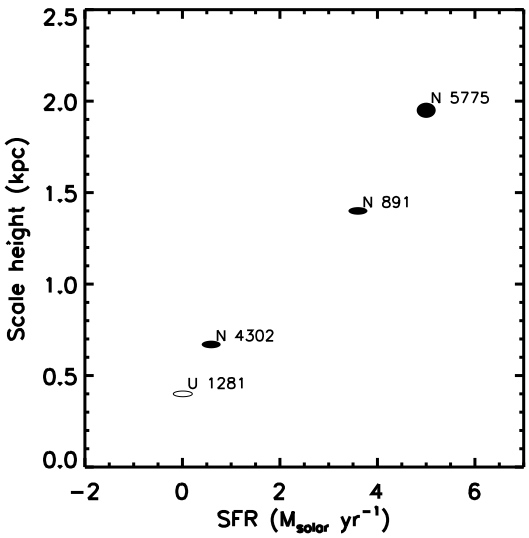

Figure 4.18: Star formation rate vs. the Hα scale height for the galaxies from Heald et al. (2007) (filled ellipses) and UGC 1281 (open ellipse). The vertical axis of an ellipse indicates the error in scale height for a specific galaxy

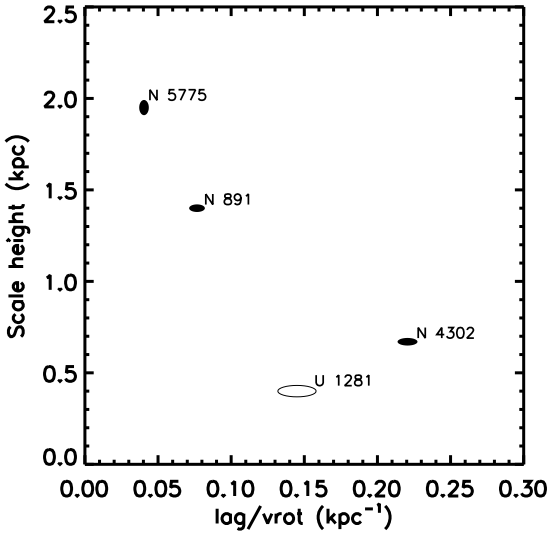

Figure 4.19: Lag/v_{max} vs. the Hα scale height for the galaxies from Heald et al. (2007) (filled ellipses) and UGC 1281 (open ellipse). The horizontal (vertical) axis of an ellipse indicates the error in lag/v_{max} (scale height) for a specific galaxy

likely caused by the fact that UGC 1281 is a dwarf galaxy whereas the galaxies compared by Heald et al. (2007) are massive. This seems to indicate that the lag does not always scale solely with the scale height of the ionized gas. If the lag is mostly caused by star formation one would expect this relation to hold everywhere since the scale height of the ionized gas is correlated to the SFR of a galaxy (See Fig. 4.18).

Not only is the vertical gradient expected to correlate with the SFR, but also with the overall size of the galaxy.

If we look at the ballistic model for UGC 1281 we already find a much lower predicted vertical gradient of 0.4 km s^{-1} kpc^{-1} than in the ballistic models for the bigger galaxies (1-4 km s^{-1} kpc^{-1}, Heald et al. (2007), see § 4.5.2). However, the ballistic model is not equally applicable to UGC 1281 because of its small scale height, and therefore only an absolute upper limit on the lag can be achieved with ballistic models.

A different way to investigate whether the overall size influences the amount of vertical gradient observed, is to scale the lag by a parameter which is known to be tied to the overall size of a galaxy. Figure 4.19 shows the lag in each galaxy divided by the maximum rotational velocity v_{max} plotted against the Hα scale height. It is clearly seen that now there is a correlation between NGC 891, NGC 5775 and UGC 1281. However, NGC 4302 is now the outlier instead of UGC 1281.

The previous discussion clearly shows the need for investigation of the lag in a much larger sample than the one that has been available up to now.

A warp

The other possibility is that UGC 1281 does not have any halo at all or a non-lagging halo and that it is just the warp that is causing the apparent lag. Warps are quite common in disk galaxies and often they are asymmetric (García-Ruiz et al. 2002) as is observed for UGC 1281. If the extra-planar HI and its kinematics in UGC 1281 is to be fully explained by a warp, the warping axis has to have an angle of 35° with respect to the line of sight.

We would like to point out the very small differences between the lagging halo model (Model D) and the maximum line of sight warp model (Model F). The maximum difference in inclination between the two models is 3° which results in a difference in scale height of $\sim 1''$ (See Figure 4.12). Also this small difference takes away the need for a lag. This once more shows that it is very hard to separate between line of sight warps and lagging halos and that great care must be taken to exclude one of the two options.

When we measure once more the maxima in normalized PV diagrams parallel to the minor axis we find an apparent lag of 5.5±1.2 km s^{-1} kpc^{-1}, for a model with the maximum line of sight warp (Model F), which is consistent with the measurement from the data (6.3±2.1 km s^{-1} kpc^{-1}). Therefore there is no need to introduce a lag or radial inflows in this model.

The best fit model (Model F) for this case has central scale heights which are similar to those measured from the stars and the Hα. This would mean that the stars and the ionized gas hardly extend into the warped regions of the disk and that all the extra planar HI is in the warp and flare.

This is consistent with the findings of van der Kruit (2007) that warps start just beyond the truncation radius of the stellar disk. van der Kruit (2007) discuss as possible

warp origin a two-stage evolution for disk galaxies. In the first stage the flat inner stellar disk is formed with a gas disk of similar size. The extended and warped parts of the gas disk are then formed in a later stage by the accretion of gas from the inter galactic medium (IGM) with higher angular momentum than the initial disk.

However, from the modeling and the observed structure we know that there is some warped gas within the truncation radius of UGC 1281. Even more so, we know from the observed Hα emission that also the ionized gas is slightly warped (See 4.4.1). This would imply that if the warp in UGC 1281 is formed by the accretion of gas from the IGM its initial disk was not rigid enough to stabilize the infalling gas. If so, one would expect a clear difference between the onset of the warp, with respect to its truncation radius, between dwarf galaxies and massive galaxies.

4.7 Summary

We presented emission in 21 cm and Hα emission of the edge-on dwarf galaxy UGC 1281. This is the first time such sensitive HI data have been presented for a dwarf edge-on.

The integrated Hα velocity map shows a non-smooth distribution on the major axis with several peaks. One of these peaks is actually located beneath the major axis. It is unclear whether this HII region is actually located in the halo of the galaxy or in the warped outer parts.

The integrated HI velocity map shows a quite regular distribution with its most remarkable feature a central depression. This central depression appears symmetrically in position around the center but is much deeper on the NE side of the galaxy. This is typical for dwarf galaxies.

Furthermore this map shows that UGC 1281 is warped in its outer parts and this warp resembles a w shape. The warp deviates at maximum 6° in PA from the major axis and this maximum deviation occurs at about half of the total radius of the HI distribution and not in the outer parts.

For the interpretation of the kinematics of the extra-planar HI gas we constructed velocity maps from the Hα and HI data. Also 3-D models with a modified version of GALMOD are constructed in GIPSY. This modified version enables us to construct kinematic models. As a starting point for the HI model we used the observed radial and vertical distribution and a rotation curve obtained from the 1st moment map. Then the model is iterated (by hand) until a best fit is obtained.

The rotation curve obtained from the best fit models shows a slow rise in its inner part. This is also seen in the velocities obtained directly from the data and therefore unlikely to be an effect of the HI distribution or resolution. At about 120″ the rotation curve flattens off to a maximum rotational velocity ~ 60 km s^{-1}. This slow rise is seen in many dwarf galaxies and thought to be caused by a dark matter dominated mass distribution.

From our modeling we find that our data is not sensitive enough to distinguish between a lagging halo or a line of sight warp. Both models fit the data equally well and there is only a small difference between the input parameters of the models.

In the case of a lagging halo the low vertical extent and the low flux level of the Hα

emission would indicate that this extra-planar HI does not originate from galactic fountains but is either infalling primordial HI or brought up from the plane in an interaction with another galaxy.

To obtain the lag in this case we measure the apparent lag in the data by fitting the position of the maxima in normalized PV-diagrams parallel to the minor axis in the data with a straight line. Such a measurement will be affected by beam smearing and the warp and therefore we repeat this measurement for our best fit halo model covering a range in lag. This way we find that the vertical velocity gradient in UGC 1281 in the case of a lagging halo is 8.7 ± 4.1 km s^{-1} kpc^{-1}.

Great care must be taken to distinguish between lagging halos and line of sight warps since small changes in the modeling can have a great effect on the velocity field.

In the case of a line of sight warp the ionized hydrogen and the distribution of the stars would not extend into the warped region of the disk. However, the scale height in the central parts would be the same for the stars, Hα and HI.

Summarising our main conclusions:

- The rotation curve of UGC 1281 is slowly rising in its inner parts and flattens off to a maximum rotational velocity ~ 60 km s^{-1} at $120''$ (3.14 kpc).
- The neutral hydrogen in UGC 1281 is more extended than the stars and the ionized emission in its radial distribution.
- Our observations can be fitted by both a lagging halo and a line of sight warp. The observations are not sensitive enough to separate between these two options.

Acknowledgements

We thank R. Kuzio de Naray for making her velocity data available to us. We are grateful to S. Sanchez and A. Guijarro for doing the PPAK observations and M. Verheijen for introducing us to PPAK. Many thanks to T. Oosterloo for help with the HI data reduction and to P. Serra for useful discussion and insights.